To Mix or Not To Mix: 2D Crystallization and Mixing Behavior of Saturated and Unsaturated Aliphatic Primary Amides

Kunal S. Mali,[†] Bernard Van Averbeke,[‡] Tej Bhinde,[§] Adam Y. Brewer,[§] Thomas Arnold,[⊥] Roberto Lazzaroni,[‡] Stuart M. Clarke,[§] and Steven De Feyter[†,*]

[†]Division of Molecular Imaging and Photonics, Department of Chemistry, Katholieke Universiteit Leuven, Celestijnenlaan 200F, B 3001, Leuven, Belgium, [‡]Service de Chimie des Matériaux Nouveaux, Université de Mons, 20 Place du Parc, B-7000 Mons, Belgium, [§]BP Institute and Department of Chemistry, University of Cambridge, Madingley Rise, Madingley Road, Cambridge CB3 0EZ, United Kingdom, and [⊥]DIAMOND Light Source Ltd., Diamond House, Harwell Science and Innovation Campus, Chilton, Didcot, Oxfordshire OX11 0DE, U.K.

ABSTRACT Physisorbed monolayers based on relatively weak noncovalent interactions can serve as excellent model systems for understanding crystallization of materials in reduced dimensionality. Here we employ a powerful combination of scanning tunneling microscopy (STM), differential scanning calorimetry (DSC), and computational modeling to reveal two-dimensional (2D) crystallization and mixing behavior of saturated and unsaturated (*cis* as well as *trans*) aliphatic primary amides. The foundation of the present work is laid by DSC measurements, which reveal characteristic adsorption and mixing behavior of aliphatic amides. These results are further supported by STM visualization of the adlayers. STM reveals, at submolecular resolution, the adsorption as well as the two-component 2D phase behavior of these molecules at the liquid–solid interface. The saturated and *trans*-unsaturated amides exhibit random mixing in view of their size and shape complementarity. Binary mixtures of saturated and *cis*-unsaturated amides, on the other hand, display unprecedented mixing behavior. The linear saturated and bent *cis*-unsaturated amide molecules are found to mix surprisingly better at the liquid–solid interface than might have been expected on account of the dissimilarity in their shapes. Strong, directional intermolecular hydrogen-bonding interactions as well as the relative stabilization energies of the adlayers are responsible for such unusual mixing behavior. Computational modeling provides additional insight into all the possible interactions in 2D assemblies and their impact on stabilization energies of the supramolecular networks. This study provides a model for understanding the effect of nanoscale cocrystallization on the thin film structure at interfaces and demonstrates the importance of molecular geometry and hydrogen bonding in determining the coadsorption behavior.

KEYWORDS: mixing behavior · cocrystallization · STM · DSC · liquid–solid interface · MM/MD simulations

The phenomenon of crystallization is of immense scientific and technological importance in view of the fact that various functional properties of materials are ultimately determined by the way in which molecules pack in crystals. Despite intensive research, a generalized method for understanding crystallization simply based on the molecular formulae has proved to be illusive for more than 50 years.[1−3] The crystal structures of molecular substances, particularly organic compounds, are extremely difficult to predict because the factors that determine them—the intermolecular interactions—are numerous, weak, and have little directionality. One of the promising approaches is to study the crystallization problem in a reduced dimensionality. Two-dimensional (2D) crystalline monolayers based on physisorbed molecules at the liquid–solid interface have served as excellent model systems for understanding crystallization of materials in reduced dimensionality.[4−8] Such 2D crystals can often be useful to comprehend the selection of one possible polymorph over the other and also in predicting the adsorption from multicomponent solutions.[9] In fact, crystallization of mixtures forming multiple phases is commercially important, since such mixtures often offer either reduced cost or enhanced performance relative to pure materials.[10] An advantage of studying such multicomponent systems at reduced dimensionality is that phases that are not fully periodic and are adsorbed at the "buried" and experimentally inaccessible liquid–solid interface can be readily examined by employing scanning tunneling microscopy (STM)[4−8] and in-plane diffraction techniques,[11−13] offering structural and mechanistic insights at submolecular resolution.

Since a great deal of information can be obtained about molecular ordering through STM investigation of 2D crystals, numerous studies have focused on the self-assembly of organic molecules on atomically flat conductive substrates such as highly oriented

* Address correspondence to Steven.DeFeyter@chem.kuleuven.be.

Received for review August 31, 2011 and accepted October 10, 2011.

Published online October 19, 2011
10.1021/nn203358x

pyrolytic graphite (HOPG) and Au (111).[4−8] Typical intermolecular bonding motifs encountered in 3D crystallization processes such as the ones sustained by van der Waals forces, hydrogen bonding, metal coordination, and dipole−dipole and electrostatic interactions have also been utilized to form well-defined 2D monolayers on surfaces.[14] Thus, structural characterization of the solution-formed physisorbed monolayers assumes special importance, as it allows us to probe the fundamental aspects of the self-assembly events leading to nucleation and crystal growth. Moreover, such adlayers mimic the organization of molecules on a substrate during lubrication,[15,16] fabrication of thin film organic electronic devices,[17] and surface coatings.[18] A precise understanding of the assembly mechanisms and phase behavior of such self-assembled monolayers is critical for understanding how their structure/function properties arise.

One of the fundamental issues in this context is that of coassembly: this revolves around the two-component 2D phase behavior of a system when two different species undergo 2D crystallization on a single substrate. This issue has been addressed in numerous STM investigations,[6,19−52] and coadsorption of as many as four different components has been accomplished *via* "2D crystal engineering".[50] An overview of various STM investigations carried out so far reveals that when a multicomponent solution is brought in contact with a solid substrate, it can lead to coadsorption, which can manifest as: (1) Phase separation[19−24] on the nanometer scale, which occurs when both the components adsorb; however, each component adopts a structure that is identical to that obtained from the pure solution. Thus, each component is confined to a distinct domain. For example, *n*-tetracontane ($C_{40}H_{22}$) and 4′-octyl-4-cynobiphenyl (8-CB) crystallize in different domains due to dissimilarity in the size of the molecules and incompatible functional groups.[22] (2) Formation of randomly mixed monolayers.[25−32,53] Such mixed monolayers are formed when one component is incorporated into the crystal lattice of the other in a nonperiodic fashion. For example, molecules of (*E*)-octadec-9-enoic acid are inserted randomly into the crystallized monolayer of octadecanoic acid without disruption of the original self-assembled monolayer because these two molecules crystallize into identical unit cells.[29] (3) Cocrystallization into highly ordered 2D bimolecular crystals.[6,33−52] A cocrystal is formed when one component inserts into a crystal of another in a repeating pattern, giving rise to a new bimolecular crystal. Typically, cocrystallization is a result of strong intermolecular interactions such as hydrogen[40−42] or halogen[54] bonding or space-filling constraints as observed in 2D host−guest systems.[6] The general consensus that emerged from such experiments indicates that the mixing behavior at the liquid−solid interface strongly depends upon both the symmetry and the quantitative similarity of the unit cells as well as the compatibility of functional groups.[4,55]

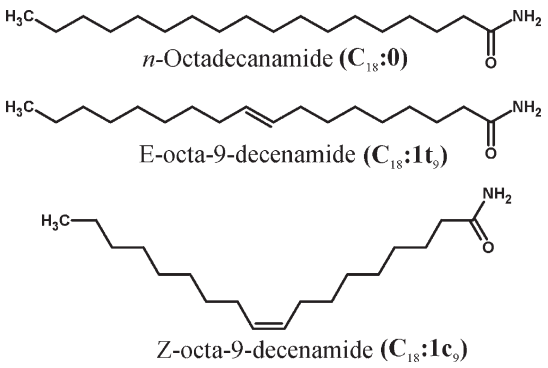

Scheme 1. Chemical structures of the amides used in this study.

In this contribution, we report on 2D crystallization and mixing behavior of simple aliphatic saturated and unsaturated primary amides (Scheme 1). Primary alkylamides have several important commercial applications that exploit their behavior at interfaces. One of the typical applications is their use as friction modifiers for rough polymer films that exhibit a high coefficient of friction.[56] These materials are frequently derived from plant sources and usually consist of mixtures within a single usable material. It is well known that the presence of small amounts of unsaturated impurities can have a dramatic impact on material properties such as the melting point. Thus, considering the importance of materials used as surface coatings in general, it is important to understand the 2D crystallization and the effect of mixing on the nanoscale (co)adsorption. As a first step in that direction, the crystalline structures of saturated alkylamide monolayers adsorbed on the graphite surface have been elucidated recently by using synchrotron X-ray and neutron diffraction techniques.[12] In addition to this, a detailed thermodynamic investigation[57] carried out in the recent past revealed that saturated and unsaturated (*cis* as well as *trans*) amides mix rather better than might have been expected on the basis of their shapes.[57]

The differential scanning calorimetry (DSC) data suggested that the binary mixture of *trans*-unsaturated and saturated amides exhibits significant nonideality in the mixing, but no phase separation occurs. On the other hand, the thermodynamic data on the binary mixture of *cis*-unsaturated and saturated amides were less clear. Given the experimental uncertainities and pronounced asymmetry of the phase diagram, it could not be ascertained if the system displayed nonideal mixing or phase separation.[57] Therefore, in order to get a clearer idea about the mixing behavior of this system, STM operating at the liquid−solid interface was employed as a complementary tool. With this approach one can directly observe the molecular organization on surfaces in real space and real time. In contrast to DSC,

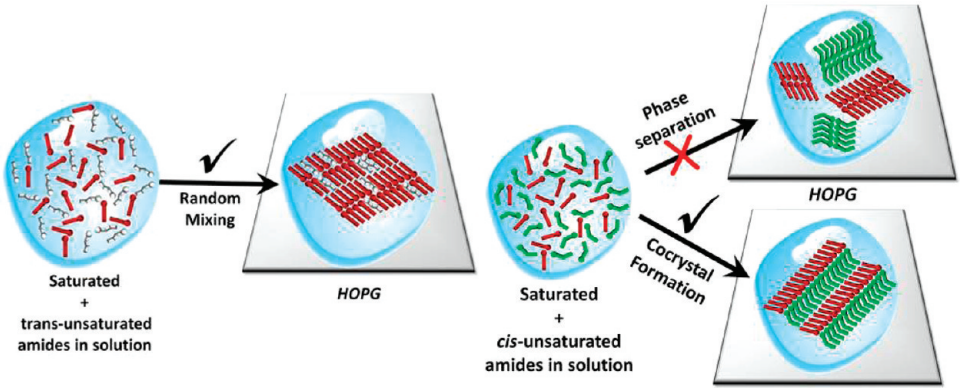

Scheme 2. Schematic showing the summary of the mixing experiments performed in this study.

which integrates information obtained over large areas, STM provides information at the single-molecule level, and one can probe the molecular organization locally.

Thus, in the present study, we exploit the high spatial resolution of STM to scrutinize the adsorption and mixing behavior of aliphatic amides. The STM data are supported by molecular modeling (MM) simulations, which provide an atomistic and energetic insight into the formation and stabilization of the amides and their mixtures. In essence, the salient features of this study are the following: (1) detailed STM characterization of the saturated and unsaturated alkylamide monolayers at high spatial resolution, which is an essential step in comprehending the mixing behavior. (2) STM visualization of a monolayer composed entirely of the *cis*-unsaturated isomer. Although the *trans*-isomer-based monolayers have been visualized routinely at submolecular resolution, monolayers entirely composed of *cis*-isomers could rarely[58−60] be observed at the solid−liquid interface. This has been attributed to desorption of molecules due to the inability to pack efficiently. The *cis*-unsaturated amides form stable monolayers, which could be observed at high resolution using STM. (3) competitive adsorption and random mixing behavior in the mixed adlayers of saturated and *trans*-unsaturated amides and (4) unprecedented mixing behavior of linear and bent molecules. Experiments carried out in the past indicate that linear and bent rodlike molecules do not mix. For example, the linear saturated fatty acid, stearic acid (octadecanoic acid) and the bent *cis*-unsaturated oleic acid (*Z*)-9-octadecanoic acid do not form a solid solution at any composition ratio since it is difficult to pack these geometrically dissimilar rodlike molecules.[61] In contrast, the results reported here demonstrate an unprecedented mixing of saturated and *cis*-unsaturated amides in 2D. The coadsorption behavior described here does not conform to any of the cases reported earlier, since the mixing experiments reported so far utilized molecules that exhibited shape complementarity. In the present case, the *cis*-isomer has a significant bend in the alkyl chain as compared to the saturated and *trans*-unsaturated molecules, which are essentially linear molecules. When combined in solution in a narrow range of ratios, the linear and bent molecules gave rise to different types of mixing patterns ranging from phase-separated columns to cocrystals. Formation of cocrystals in these 2D binary mixtures is both unexpected in light of the structural dissimilarity of the constituent molecules and unusual, considering the inherent instability associated with the 2D crystallization of *cis*-isomers. Examples of such anomalous mixing behavior can be found in nature such as the lipid "rafts" in cell plasma membranes in which submicrometer domains of sphingolipids, which contain mostly long-chain saturated acyl chains, coexist with glycerophospholipids that consist of *cis*-unsaturated acyl chains with a bent structure.[62−64] The results presented here are thus important in this context as well since a variety of biological functions have been attributed to such mixed structures.[62,63] A summary of the mixing experiments carried out in the present work is shown graphically in Scheme 2.

RESULTS AND DISCUSSION

2D Crystallization from Monocomponent Solutions. The hydrogen-bonding energy associated with dimerization of bulk amides in solution is between 10 and 20 kJ/mol.[65,66] In contrast, typical van der Waals interaction energies between adsorbed alkylated molecules reflected in the melting heats of alkanes on graphite are ~7 kJ/mol.[67] Thus, the 2D ordering of amides is expected to be controlled by the stronger and more directional hydrogen bonds. Considering the hydrogen-bonding ability of a primary amide group, two different types of hydrogen bonds prevail in these adlayers. "Intradimer" and "interdimer" hydrogen bonds are formed within a single dimer and between adjacent dimers, respectively (Supporting Information, Figure S1). It is this extensive "head-on" and "lateral" hydrogen bonding that makes the amide monolayers much more stable compared to other alkylated species.[12,57]

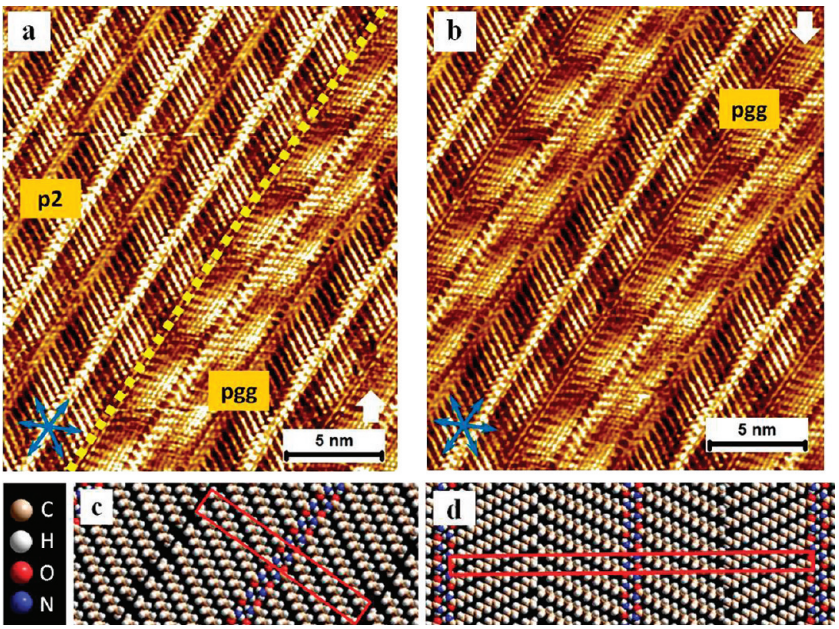

Figure 1. High-resolution (HR) STM images of the 2D crystallized C_{18}:0 amide at the 1-phenyloctane−HOPG interface. (a) STM images depicting the coexistence of *p2*- and *pgg*-type packing. (b) *pgg*-type packing. The blue arrows in the lower left corner indicate the main symmetry axes of graphite. Imaging conditions: I_{set} = 175 pA, V_{bias} = −750 mV. (c and d) Tentative packing models for the *p2*- and *pgg*-type structures, respectively. The unit cell is depicted on the molecular models.

Figure 1 shows STM images of a 2D monolayer of *n*-octadecanamide (**C_{18}:0**) physisorbed at the 1-phenyloctane/HOPG interface. **C_{18}:0** crystallizes into a columnar pattern in which the molecules form hydrogen-bonded dimers with their alkyl backbones lying parallel to the surface of HOPG in a non-interdigitated fashion. The columnar structure accommodates both hydrogen bonding between the amide functional groups and van der Waals interactions between the alkyl chains within a column. STM images displayed in Figure 1 indicate that the amide functional groups appear with brighter contrast relative to the alkyl backbones of the molecules. However, some STM images (Supporting Information, Figure S4) indicate that the amide groups can also exhibit darker contrast relative to the alkyl chains. Such contrast variation of different functional groups has been systematically studied by Flynn *et al.*[68] They observed that the contrast of the amide groups varies as a function of applied substrate bias. However, our results illustrate that apart from the tunneling conditions, the shape of the STM tip apex also strongly governs the apparent height of functional groups in STM images, since we could observe the "bright" as well "dark" contrast of the amide groups under identical tunneling conditions (Supporting Information, Figure S4). The alkyl chains are fully extended, compactly packed, and aligned along one of the symmetry axes of graphite lattice. The width of the column is 4.68 ± 0.05 nm. The orientation of the alkyl chains with respect to the column propagation axis is 61.3 ± 0.9°, and these molecular columns in turn make an angle of 1.8 ± 0.7° with one of the principal symmetry axes of graphite. The molecules are separated by 0.50 ± 0.01 nm along the column axis, and the distance between alkyl backbones, measured perpendicular to the chain orientation, is 0.45 ± 0.01 nm, which correlates reasonably well with the distance observed between long-chain alkanes adsorbed on graphite.[69] A striking feature of the STM images depicted in Figure 1 is the strong contrast modulation along the column. This modulation arises from the moiré pattern, which is attributed to the near, but not perfect commensurate packing of the molecules with respect to the graphite lattice along the column. This minor mismatch creates an interference effect between the alkyl backbones of the molecules and the underlying substrate lattice, modulating the tunneling current.[69−71]

The STM images displayed in Figure 1 clearly exhibit two different types of packing patterns. These two types correspond to collinear dimers in adjacent columns or non-collinear dimers in the adjacent columns (herringbone-type pattern). The non-collinear dimers in adjacent columns are related by 60° rotation along the long molecular axis. These packings give rise to structures with two possible plane groups: *p2* with 2 molecules/unit cell and *pgg* with 4 molecules/unit cell. Molecular models that reproduce the observed metrics and symmetry in the STM images are displayed in Figure 1c,d. The unit cell parameters for the *pgg* as well as *p2* symmetric adsorption patterns obtained from STM as well as from MM calculations are given in Table 1 and are in close agreement. This structural behavior, which gives rise to two dissimilar types of

TABLE 1. Experimental and Computed Lattice Parameters for the 2D Crystallized Adlayers of Alkylamides

			unit cell parameters (STM)			unit cell parameters (molecular modeling)		
amides	plane group	molecules/unit cell	*a* (nm)	*b* (nm)	α (deg)	*a* (nm)	*b* (nm)	α (deg)
C_{18}:0	*p2*	2	4.73 ± 0.03	0.50 ± 0.01	87.5 ± 1.0	4.86 ± 0.04	0.52 ± 0.03	94 ± 3
C_{18}:0	*pgg*	4	9.48 ± 0.02	0.51 ± 0.01	90.1 ± 1.2	9.64 ± 0.03	0.52 ± 0.02	90 ± 3
C_{18}:1t_9	*p2*	2	4.72 ± 0.04	0.51 ± 0.01	88.0 ± 1.5	4.79 ± 0.08	0.52 ± 0.03	88 ± 3
C_{18}:1c_9	*p2*	2	4.66 ± 0.03	0.51 ± 0.01	88.5 ± 1.6	4.80 ± 0.04	0.52 ± 0.02	90 ± 2

TABLE 2. Energetics (kJ mol^{-1} molecule^{-1}) of the 2D Crystalline Adlayers of Amides Obtained from Molecular Modeling

		C_{18}:0			
		p2	*pgg*	C_{18}:1t_9	C_{18}:1c_9
total potential energy		−22.57	−22.13	−20.35	−1.3
van der Waals term	2D assembly	89.34	87.60	86.39	92.83
	surface interaction	−175.59	−175.03	−171.1	−171.06
electrostatic term		−127.52	−127.26	−127.18	−127.83
hydrogen bond term		−21.05	−20.35	−20.75	−20.31

packings, has been predicted earlier from X-ray and neutron diffraction experiments.[12] The free energy difference between the two packings (*p2* and *pgg*) is rather small, and the change in the plane group symmetry arises due to subtle differences in the interactions between the terminal methyl groups. STM images of **C_{18}:0** further reveal that the occurrence of the *pgg* symmetric structure is rather sparse in comparison with the *p2* symmetric structure. In fact, *ex-situ* annealing of the sample at 45 °C for 10 min led to complete change of the monolayer morphology. The *pgg* packing could no longer be visualized, and the entire surface was exclusively covered with relatively large domains of *p2*-type packing (Supporting Information, Figure S5). Moreover, once the rearrangement to the *p2* symmetric packing was complete, the system did not revert back to the *pgg* packing even after several hours. This implies that the *pgg* network represents a kinetically trapped structure that gets transformed into thermodynamically more stable *p2* packing upon heating. The calculated lattice stabilization energies of the *p2* and *pgg* symmetric structures displayed in Table 2 also reveal that the *p2*-type packing has a slight edge over *pgg*.

Although (*E*)-octa-9-decenamide (**C_{18}:1t_9**) possesses a double bond, the *trans*-geometry ensures that the segments on either side of the double bond are essentially collinear, and hence the shape of the molecule is almost straight. The molecule, however, appears kinked in the STM images due to the presence of the double bond in the middle of the backbone. It has been argued in the recent past that such unsaturation has a destabilizing effect on the monolayer relative to the saturated system, and the destabilizing effect of a *trans*-double bond is less than its *cis*-counterpart.[57]

Figure 2 shows STM images of the surface crystallized monolayers of **C_{18}:1t_9** at the 1-phenyloctane−HOPG interface. While the adlayer structure resembles the *p2*-type packing (Figure 1a,c) observed in the case of **C_{18}:0**, the appearance of **C_{18}:1t_9** molecules is distinctly different than those of **C_{18}:0**. The molecules exhibit a bright kink in the middle, as expected from the *trans*-geometry of the double bond. A close inspection of the STM images reveals that three rows of bright features appear along the length of the column. Two of them (gray arrows in Figure 2b) originate from the double bonds of the molecules,[71,72] whereas the middle bright row (green arrow) appears at an approximate location of the hydrogen-bonded amide functionalities. However, the central bright row is slightly off-center and appears to be located at the end of only one row of molecules along the column axis. Considering the fact that the amide groups exhibit varying contrast, it is not straightforward to attribute the central row of bright features to the hydrogen-bonded amide groups. Such unusual contrast features might be caused by some scanning artifact, which could also account for the apparent difference in the length of the molecules adsorbed in the same column. A tentative molecular model is displayed in Figure 2c to aid visualization of the packing structure in this 2D crystal. The column width is 4.66 ± 0.06 nm, and the molecules in each column are oriented at an angle of 60.5 ± 2.0° with respect to the column axis. The molecular columns in turn are oriented at about 1.6 ± 1.0° with respect to the symmetry axes of HOPG. The experimentally obtained and computed unit cell parameters of **C_{18}:1t_9** are given in Table 1. The lattice parameters for **C_{18}:1t_9** and **C_{18}:0** systems are somewhat identical in view of the identical size and shape of the constituent molecules.

In contrast to the *trans*-conformation of the −CH═CH− group, the *cis*- conformation switches the extension direction (on either side of the double bond) of the carbon skeleton by 120°. As mentioned earlier, such nonlinear conformation of the molecule possibly induces destabilization in the monolayer network due to the inability of the molecules to pack efficiently. Consequently, very few examples have been reported on the STM visualization of molecules possessing a *cis*-double bond.[58−60] Bernasek *et al.*[60] studied the influence of odd−even effects in the carbon skeleton of

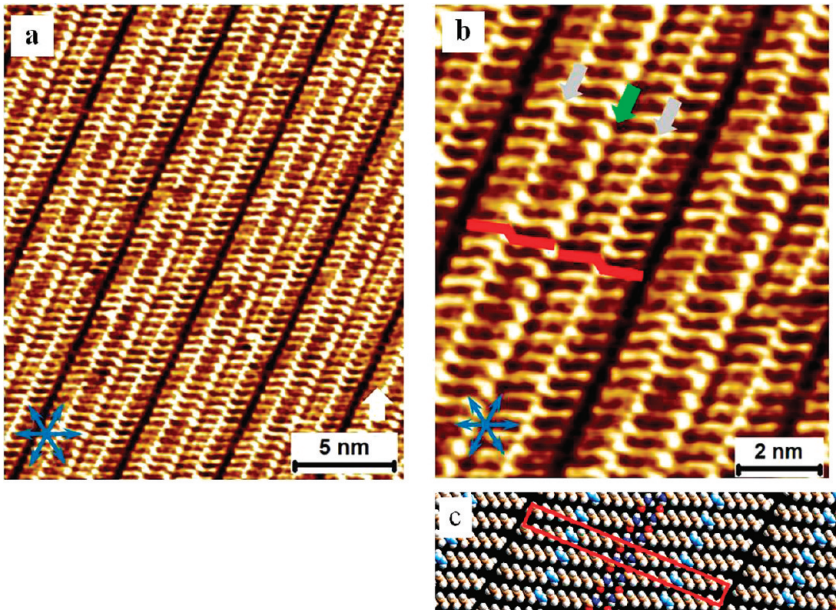

Figure 2. (a and b) HR-STM images of the 2D crystallized C_{18}:1t_9 amide at the 1-phenyloctane–HOPG interface. Two molecules of C_{18}:1t_9 are indicated schematically in red in part (b). The green arrow in (b) indicates the location of the amide headgroups, whereas the gray arrows indicate the positions of the double bonds along the molecular column. Imaging conditions I_{set} = 186 pA, V_{bias}= −800 mV. (c) Tentative packing model for the observed structure (C═C shown in light blue).

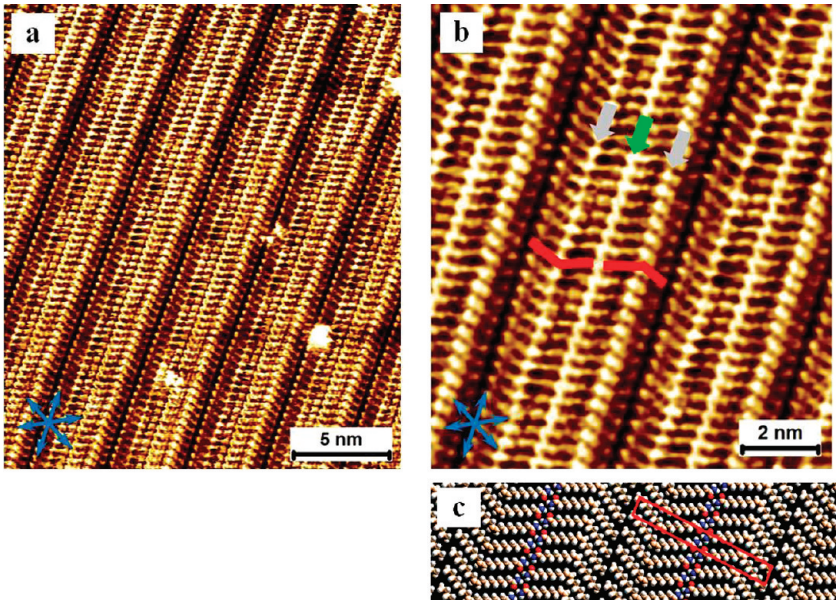

Figure 3. (a and b) High-resolution STM images of the 2D crystallized C_{18}:1c_9 amide at the 1-phenyloctane–HOPG interface. Two molecules of C_{18}:1c_9 are indicated schematically in red in part (b). The green arrow in (b) indicates the location of the amide headgroups, whereas the gray arrows indicate the positions of the double bonds along the molecular column. Imaging conditions: I_{set} = 160 pA, V_{bias} = −850 mV. (c) Packing model for the observed structure.

various *cis*-unsaturated carboxylic acids on the self-assembly at the organic solvent–HOPG interface. Stable monolayers were observed for various *cis*-acids, and the stability of the self-assembled networks was ascribed to the formation of hydrogen bonds between molecules.[60] Thus, considering the hydrogen-bonding pattern in primary amides, one readily expects them to form relatively more stable monolayers than carboxylic acids since the hydrogen bond density is higher in the former in view of extensive "lateral" hydrogen-bonding interactions as described earlier.

Figure 3 shows the STM images of (*Z*)-octa-9-decenamide (**C_{18}:1c_9**) adsorbed on HOPG surface from 1-phenyloctane solution. **C_{18}:1c_9** also crystallizes in a columnar packing in which the "bent-knee"-shaped molecules are arranged compactly along the column axis. *cis*-Double bonds appear as a characteristic bright ridge along the column propagation direction. The

alkyl chains on either side of this ridge make an angle of ~120° with each other, as expected from the *cis*-geometry of the double bond. In fact, the 3-fold symmetry of the underlying graphite lattice allows epitaxial adsorption of the molecular skeleton containing two all-*trans* alkyl chains with an angle of 120°. The tail (methyl end containing) segments of the molecules appear with a darker contrast relative to the rest of the molecule. This effect is somewhat similar to that observed in the case of **C_{18}:1t_9**. As mentioned already, such effects could arise due to experimental artifacts, or alternatively they could be associated with the presence of double bonds in the backbones, which slightly lift the terminal regions of the chains from the surface, thus affecting the electronic coupling between the substrate and molecules. Despite a significant bend in the molecule, the column width in the case of **C_{18}:1c_9** (4.65 ± 0.06 nm) is very similar to that of **C_{18}:0**, which is essentially a straight molecule. The molecules are separated by 0.51 ± 0.02 nm along the column axis, and the columns are oriented at an angle of 3.0 ± 1.0° with respect to one of the principal symmetry axes of graphite. The two segments on either side of the *cis*-double bond are oriented along the symmetry axes of graphite, imparting some sort of epitaxial stabilization to the self-assembled network, as described earlier. Nevertheless, the bent shape of the molecule and the unsaturation in the molecular backbone make the **C_{18}:1c_9** adlayer relatively less stable than that formed by **C_{18}:0**.

The trend in the relative stabilities of these molecular networks, which is reflected in their monolayer melting enthalpies (ΔH_m^{2D}), indicates that fully saturated amide (**C_{18}:0**, ΔH_m^{2D} = 62.9 kJ mol^{-1}) forms the most stable adlayer followed by *trans*-unsaturated amide (**C_{18}:1t_9**, ΔH_m^{2D} = 45.9 kJ mol^{-1}), whereas the adlayer formed by the *cis*-isomer (**C_{18}:1c_9**, ΔH_m^{2D} = 39.7 kJ mol^{-1}) is the least stable among the three molecules.[57] These numbers suggest that the saturated alkyl chains help to anchor the molecules, thus enhancing the monolayer stability, whereas the double bond provides a "break" in this stability, perhaps by preventing effective packing or by slightly lifting the alkyl chains from the surface.[75] The trend observed in the monolayer melting enthalpies of these molecules is also reflected in the calculated total potential energies of their self-assembled networks. Table 2 provides lattice energies obtained from molecular dynamics (MD) simulations performed on the three systems. The procedure used for calculating these values is described in detail in the Supporting Information. It must be noted at this juncture that a direct comparison between the total energy of different systems must be treated with some caution since the chemical composition of each system is different. It is possible, however, to get an idea about the relative energetics of assemblies that have identical atomic composition (*p2* against *pgg*, *trans- versus cis*-isomer). One can also compare parameters that are independent of the chemical structure such as hydrogen bonds since the amide group is common for all three molecules. A direct comparison of *p2* against *pgg* shows that *p2* is slightly favored with respect to *pgg* even if both structures are available at room temperature. The analysis further indicates that despite a certain stability of the 2D assembly (vdW) for *pgg*, all other interactions are in favor of *p2*, making it a preferred adsorption pattern. The energies of **C_{18}:0** and **C_{18}:1t_9** are comparable, whereas the total potential energy of the **C_{18}:1c_9** adlayer is significantly smaller than that of **C_{18}:0**. The intermolecular interactions are slightly less favorable in the case of **C_{18}:1c_9** mainly for the van der Waals forces, which could be attributed to the bent shape of the molecules, which leads to less efficient packing. In addition, the simulations also indicate unfavorable contributions from valence parameters (not given here) and higher internal energy to the total potential energy for the **C_{18}:1c_9** adlayer.

2D Crystallization from Bicomponent Solutions. The STM images discussed above illustrate the structures of 2D monolayers when crystallized from a monocomponent solution, *i.e.*, when only one amide is present in solution. However, as mentioned before, adsorption from a multicomponent solution is of particular importance due to the commercial relevance of such mixed systems. Numerous industrial processes employ mixtures of different materials, and in many cases, "enhanced" performance is obtained from the mixture over either of the pure components. Here, we systematically investigate the two-component 2D crystallization of the saturated and unsaturated amides at the liquid−solid interface.

Mixture of Saturated and *trans*-Unsaturated Amides. When considering bulk (3D) binary solutions and the behavior of the monolayers (2D) adsorbed from them, the surface composition is generally different than the bulk solution. This arises from a preferential adsorption of one of the species over the other. It has been established that, when 2D crystallization occurs from a multicomponent solution of linear species that differ only in the molecular length, the longer molecules are preferentially adsorbed even if the mole fraction of the longer species is significantly lower than that of the shorter one.[74−76] Such preferential adsorption can be understood by considering the change in the entropy of the system upon adsorption of either species. When the longer species adsorbs from a mixture, a smaller number of molecules are required to cover a given surface area than when the shorter one adsorbs. This results in a smaller entropic cost in the case of the former. The preference for the longer species, however, does not hold when one compares the coadsorption from a mixture of chemically dissimilar species.

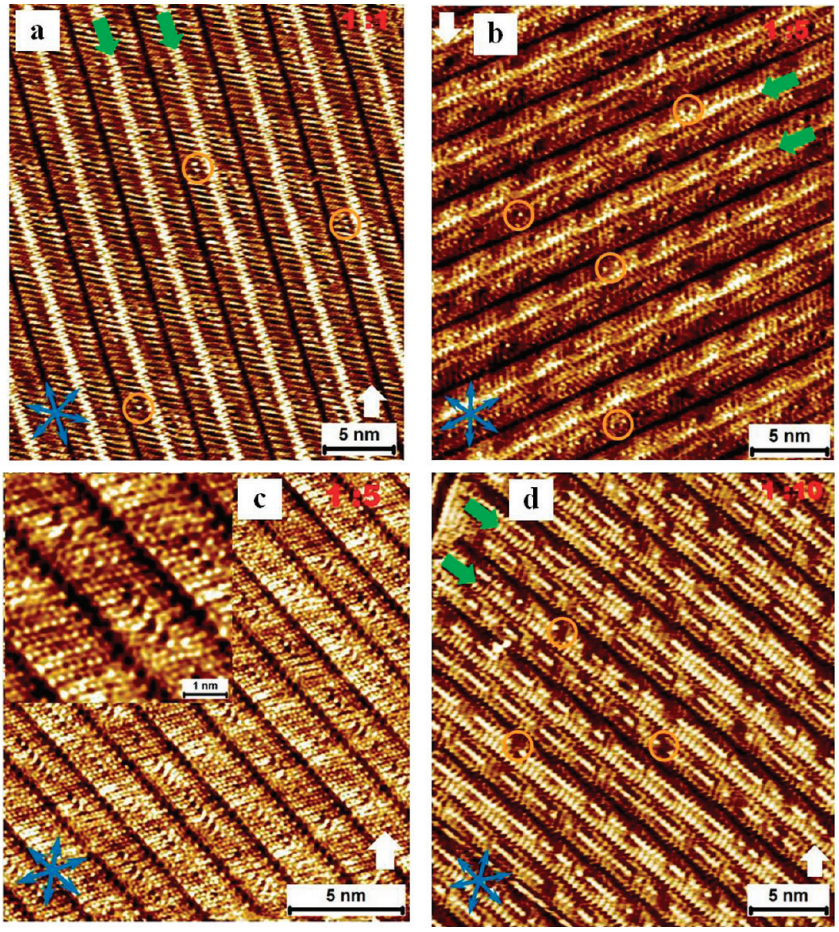

Figure 4. High-resolution STM images of the 2D crystallized adlayers formed from different mole ratios of C_{18}:0/C_{18}:1t_9 at the 1-phenyloctane–HOPG interface. Green arrows indicate locations of amide groups. (a) C_0:1t_9 = 1:1, (b and c) C_0:1t_9 = 1:5, and (d) C_0:1t_9 = 1:10. Orange circles show the bright spots along the axis except in (d), where they indicate darker features. The bright features arise due to the double bonds of the C_{18}:1t_9 molecules. Orange circles in (d) indicate the locations of C_{18}:0 molecules. Inset in (c) shows magnified area where the kinked C_{18}:1t_9 molecules could be easily identified. Imaging conditions I_{set} = 180 pA, V_{bias} = −850 mV.

For example, a shorter amide can preferentially adsorb over a longer chain alkane.[57]

Previous DSC studies on related systems have already established some general rules that predict the mixing behavior of such binary mixtures. These studies exploited the composition dependence of the monolayer melting points obtained from the DSC thermograms, which was used as an indicator of preferential adsorption (if any!) as well as the mixing within the 2D crystallized adlayers.[55] The general consensus that has emerged from these experiments reveals that, similar to the bulk, mixing in adsorbed layers depends upon the similarity in shapes of molecules, plane group symmetry, and quantitative similarity of the unit cells. A 2D isomorphism coefficient (ε), which can be used to assess and predict the extent of mixing in binary monolayers adsorbed from solution, can be defined as[55]

$$\varepsilon = 1 - \frac{\Delta}{\Gamma} \quad (1)$$

In eq 1, Δ is the area of the non-overlapping part of the two unit cells when they are superimposed so as to achieve maximum overlap, and Γ is the area due to the overlapping part. The ε value for the **C_{18}:0/C_{18}:1t_9** combination being very close to unity (ε = 0.98) predicts ideal mixing in the monolayer. The STM image in Figure 4a shows the structure of the 2D crystallized monolayer from a 1:1 molar ratio of **C_{18}:0** and **C_{18}:1t_9** amides in 1-phenyloctane. The typical features of the molecular columns visualized in the STM images are reminiscent of the adlayer formed by pure **C_{18}:0**. The 2D lattice parameters are also similar to those obtained for pure **C_{18}:0** amide. A close inspection of the STM image, however, reveals a number of bright spots scattered along the column axis and parallel to the central bright row of amide groups. These features are absent in the monocomponent **C_{18}:0** system, indicating that they arise from the **C_{18}:1t_9** molecules scattered in the monolayer. This conjecture can be further supported by the fact that double bonds (or, in general, unsaturated parts in molecules) appear bright(er) in STM images.[71,72] Moreover, these bright spots appear almost in the middle (~1.2 nm from either end) of the molecular backbone,

as expected from the position of the double bond in **C_{18}:1t_9** molecules. The random insertion of **C_{18}:1t_9** into the monolayer of **C_{18}:0** is both in line with predictions of ε value indicating essentially ideal mixing and expected from the compatibility of the functional groups as well as identical length of the molecules. A recent study that employed a combination of synchrotron X-ray diffraction and DSC has also revealed that binary mixtures of saturated and *trans*-unsaturated amides show ideal mixing in the monolayers.[70]

An unusual outcome of the present mixing experiments, however, is that despite the presence of a 1:1 molar ratio in solution, the amount of **C_{18}:1t_9** expressed in the monolayer is much smaller compared to **C_{18}:0**. This competitive adsorption behavior can be rationalized by considering the relative stabilities of the monocomponent adlayers as well as the plausible contribution from the difference in the solubility of the two amides in 1-phenyloctane. As already mentioned, ΔH_m^{2D} of **C_{18}:0** is significantly (a factor of 1.4) higher than that of **C_{18}:1t_9**. In addition, simulations also indicate slight energetic preference for the **C_{18}:0** system. This clearly indicates that when there is a competition for adsorption between the **C_{18}:0** and **C_{18}:1t_9**, the saturated analogue is adsorbed preferentially. Secondly, since these experiments have been carried out at the liquid−solid interface, one must take into consideration the relative solubilities of the two components. In general, for a successful adlayer formation at the liquid−solid interface, the solubility is expected to be intermediate in the sense that the solute should not be too soluble to hinder its 2D crystallization, and on the other hand, it should not be too insoluble since such conditions will not be favorable to bring molecules to the surface. In the present case, although both the molecules form stable adlayers from their monocomponent solutions, the solubility of **C_{18}:1t_9** in 1-phenyloctane is higher compared to that of **C_{18}:0**. In other words, the molecules of **C_{18}:1t_9** are better solvated in 1-phenyloctane than those of **C_{18}:0**, and this might be one of the factors responsible for the observed unequal expression of these molecules on the surface. This rationalization, however, is rather qualitative and must be treated with some caution.

In order to further establish the dependence of solution mole ratio on the 2D crystal composition, STM visualization of adlayers formed from 1:5 and 1:10 mol ratio (in favor of **C_{18}:1t_9**) solution was attempted. STM images displayed in Figure 4 indicate that on going from 1:1 to 1:10 mol ratio, the amount of **C_{18}:1t_9** molecules expressed on the surface increases significantly. Furthermore, when there is a 10-fold excess of the **C_{18}:1t_9** present in solution, the adlayer appears to be predominantly formed by the **C_{18}:1t_9** molecules with very few **C_{18}:0** molecules. In all cases mentioned above, the column width remains unchanged from that of the monocomponent system

TABLE 3. Energetics (kJ mol^{-1} molecule^{-1}) of the Three Possible Coadsorption Motifs for the C_{18}:0/C_{18}:1t_9 Combination

		C_{18}:0 + C_{18}:1t_9		
		phase separation	cocrystallization	random mixing
total potential energy		−14.55	−14.64	−14.77
van der Waals term	2D assembly	59.45	59.01	59.67
	surface interaction	−117.10	−117.06	−117.10
electrostatic term		−84.77	−84.69	−85.0
hydrogen bond term		−13.86	−13.65	−14.0

upon random insertion of molecules. Such random mixing behavior is observed when geometry and functionality of the two components are sufficiently compatible such that one component induces very little deformation in the crystal structure of the other.[29−31] Stevens and Beebe[29] obtained somewhat similar results from binary mixtures of stearic and elaidic acids; however, they could not comprehensively confirm the formation of randomly mixed adlayers due to lack of contrast exhibited by the *trans*-unsaturated acids. In the present case, we could identify the **C_{18}:1t_9** molecules by their distinct electronic signature in the STM images or directly through high-resolution images as depicted in Figure 4c, thus confirming their incorporation in the adlayer. Moreover, the mole ratio dependence further corroborates the random mixing of these sterically similar but electronically different molecules. In fact, comparison of the total potential energies obtained from MD simulations (Table 3) of the possible phase-separated, cocrystallized, and randomly mixed adlayers of the **C_{18}:1t_9/C_{18}:0** system illustrates that the three types of coadsorption patterns are evenly balanced and random mixing is only slightly favored over the other two modes of coadsorption. (Note here that the chemical composition is the same in all three cases, meaning that all the energetic parameters can be compared.) On the basis of the results described above, a simple mechanism can be proposed for this random mixing, which is presented in the Supporting Information (Figure S10).

Mixture of Saturated and *cis*-Unsaturated Amides. The **C_{18}:0/C_{18}:1c_9** mixture appears to be a rather incompatible combination when compared to the **C_{18}:0/C_{18}:1t_9** binary mixture. Not only do the two molecules differ in their shapes, but their lattice energies are also significantly different. The monolayer melting enthalpy of the saturated amide is ∼1.7 times that of the *cis*-unsaturated amide, whereas the total potential energy obtained from MD simulations also indicates unfavorable contributions to the adlayer of **C_{18}:1c_9**. Thus, when the mole ratio of these two molecules in solution is 1:1; the 2D crystal is indistinguishable from that formed from a pure **C_{18}:0**

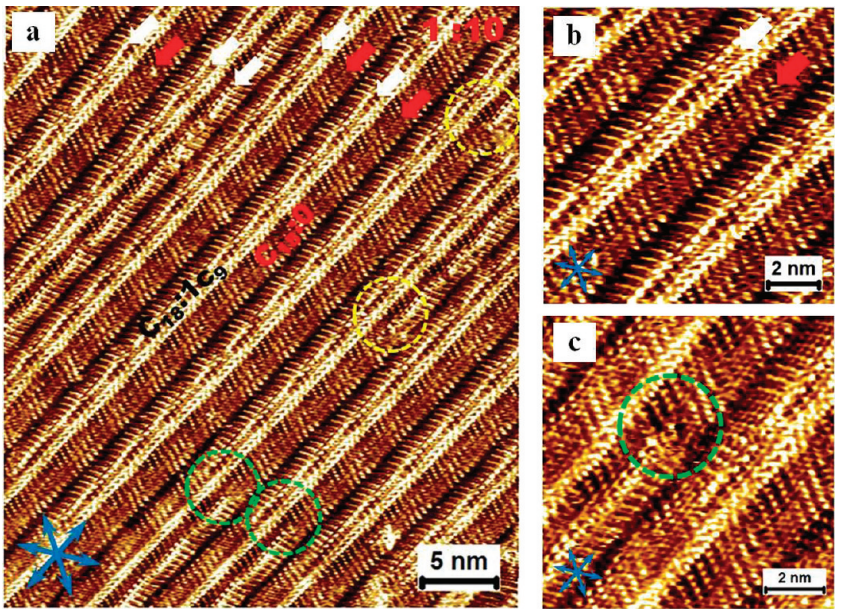

Figure 5. High-resolution STM images of the 2D crystallized adlayers formed from a 1:10 mol ratio of C_{18}:0/C_{18}:1c_9 at the 1-phenyloctane–HOPG interface. (a) STM image of the cocrystallized phase. White arrows indicate the rows of C_{18}:1c_9 molecules that are cocrystallized with C_{18}:0 molecules (red arrows). A few phase-separated columns of C_{18}:1c_9 molecules can also be visualized in the STM image. Yellow and green dotted circles indicate the locations of defect sites that are formed when the cocrystallized and phase-separated domains meet or when two cocrystallized domains with oppositely adsorbed heterodimers meet, respectively. (b) Magnified STM image showing the cocrystal and (c) magnified portion showing a defect site. Imaging conditions I_{set} = 185 pA, V_{bias} = −250 mV.

solution. In other words, the **C_{18}:0** amide is preferentially adsorbed over **C_{18}:1c_9** with a 100% preference for the former. Even as the relative amount of **C_{18}:1c_9** is increased, only the single-component **C_{18}:0** phase is formed. This behavior is in contrast to that observed in the case of the **C_{18}:0/C_{18}:1t_9** combination, wherein coadsorption of **C_{18}:1t_9** (albeit small) is observed even at 1:1 mol ratio. Apart from the large difference in the lattice stabilization energies, the lack of shape complementarity between the two molecules might be an important factor responsible for this behavior.

The ratio of **C_{18}:0/C_{18}:1c_9** in solution must be equal to or higher than 1:10 before any significant coadsorption of **C_{18}:1c_9** is observed. The STM image in Figure 5a shows the structure of the adlayer formed from a 1:10 mol ratio solution of **C_{18}:0** and **C_{18}:1c_9** amides in 1-phenyloctane. Alternate bright and dark columns could be discerned in the STM image with a clear indication that the brighter columns (indicated by white arrows) are formed by bent **C_{18}:1c_9** molecules. The columns that exhibit relatively darker contrast with striped features are attributed to the **C_{18}:0** molecular rows (red arrows). The epitaxy with the underlying graphite lattice is maintained even upon cocrystallization, though the columns in Figure 5 appear slightly distorted in comparison to those of the corresponding monocomponent systems. The width of the cocrystallized column is 4.64 ± 0.07 nm, which is identical to that of **C_{18}:1c_9** molecular columns. The characteristic "methyl group troughs" (the dark trenches in between two columns) are absent in the cocrystallized domains, thus making them relatively compact. The location of the amide functional groups in the cocrystal could not be ascertained in a straightforward manner due to the lack of specific contrast. In this scenario, two possible arrangements of the heterodimers are possible. These two cases are shown schematically in Figure 6. The amide groups in cocrystal I are collinear (facing each other), whereas in cocrystal II they form an angle at the amide junction. MD simulations of the two arrangements indicate that cocrystal II is ∼3.94 kJ mol^{-1} molecule^{-1} more stable than cocrystal I (see Table 4 for more details).

In addition to cocrystallized columns, two additional features can be noticed from Figure 5a. Phase separation is observed occasionally, though only at the level of individual hydrogen-bonded columns. A few phase-separated columns could be located in the STM image depicted in Figure 5a. Secondly, a number of defect sites (marked by dotted circles) could also be visualized. (Figure 5a,c) These defects arise either when the cocrystallized and phase-separated columns meet (yellow circles) or when two cocrystallized columns with opposite combination of hydrogen-bonded heterodimers come together (green circles) as depicted in Figure 6b. These defect sites provide another interesting situation where a linear molecule is placed next to a bent one. This situation possibly arises due to different nucleation sites on the surface, which leads to coalescence of oppositely packed heterodimer columns. The image resolution at such defect sites is relatively poor, hindering a clear identification of molecules. However,

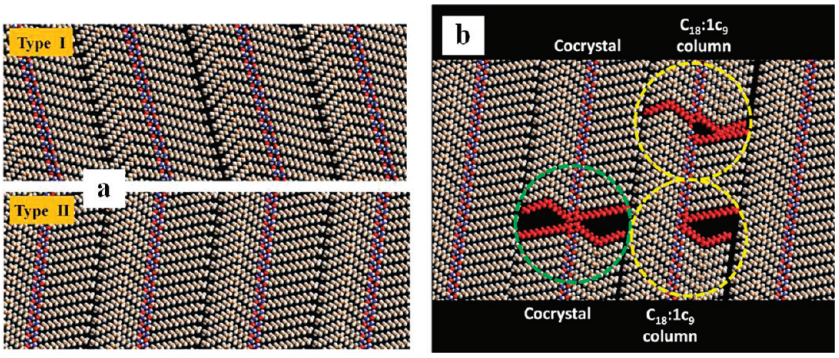

Figure 6. (a) Two possible arrangements of hydrogen-bonded C_{18}:0/C_{18}:$1c_9$ heterodimers in the cocrystallized adlayer. MD simulations indicate that the type II arrangement is ~3.94 kJ mol^{-1} molecule^{-1} more stable than type I. (b) Molecular model depicting the possible defect sites in the cocrystallized columns.

TABLE 4. Energetics of the Three Possible Crystallization Motifs for the C_{18}:0/C_{18}:$1t_9$ Combination (kJ mol^{-1} molecule^{-1})

		C_{18}:0 + C_{18}:$1c_9$		
		cocrystal I	cocrystal II	phase separation
total potential energy		−7.29	−11.23	−8.8
van der Waals term	2D assembly	90.49	92.70	92.75
	surface interaction	−175.77	−176.08	−175.46
electrostatic term		−123.70	−125.57	−124.88
hydrogen bond term		−15.68	−20.82	−20.29

the packing behavior at such defect sites could be explained by considering the 2D nature of the adlayer, where a possibility of escape in the third dimension exists. Accordingly, at such defect sites, the "tail" of a *cis*-unsaturated amide could come off from the surface, thereby increasing the available space. Thus, when combined in solution at an appropriate ratio, the linear **C_{18}:0** and bent **C_{18}:$1c_9$** molecules give rise to complex cocrystallized structures. Considering the stringent packing constraints prevalent in 2D, the coadsorption of these "shape-incompatible" molecules is rather surprising. The significant bend in the molecular structure of **C_{18}:$1c_9$** is not expected to pack well in a 2D crystal of **C_{18}:0**, which has a linear all-*trans* configuration. However, despite the lack of shape complementarity, the two types of molecules still manage to form hydrogen-bonded dimers, which in turn give rise to molecular columns *via* formation of "interdimer" hydrogen bonds. Such intimate mixing behavior is also predicted by the 2D isomorphism coefficient value for this combination, which is 0.945.

In addition to the aforementioned features, one can observe substantial adsorption−desorption dynamics in this system immediately after deposition wherein patches of **C_{18}:$1c_9$** are desorbed and re-adsorbed at a different location on the surface. This dynamic behavior can be tracked by recording time-dependent STM images in the same location on the surface of graphite (Supporting Information, Figures S11, S12). A further increase in the fraction of **C_{18}:$1c_9$** in solution (mole ratio 1:16) leads to its increased expression on the surface with concomitant displacement of the cocrystal by phase-separated **C_{18}:$1c_9$** columns (Supporting Information, Figure S11, c). However, even at this high mole ratio, small patches of cocrystallized phase are observed, indicating its favored adsorption.

The anomalous mixing behavior presented above can be understood by considering the following aspects. In general, geometrically dissimilar species are expected to phase separate, which may be seen as a default behavior when conditions of compatibility are not satisfied. The interfacial energy at the domain edge, also known as line tension, is a key parameter in determining the extent of phase separation as well as domain size. Line tension is the 2D analogue of surface tension and is defined as the free energy per unit length associated with the boundary between two phases on a surface.[77] In the present case, the line tension is expected to provide the driving force for the formation of large patches of phase-separated species. However, the very small extent of phase separation observed here indicates that the magnitude of line tension could be negligible. This behavior is reasonably consistent with the calorimetry data reported earlier on this system.[57] In addition to this, one may also consider the stability of the cocrystal with respect to either the phase-pure **C_{18}:0** or **C_{18}:$1c_9$** adlayer. At 1:1 mole ratio, the phase-pure adlayer of **C_{18}:0** outcompetes the cocrystal as well as **C_{18}:$1c_9$** adlayer. The pure **C_{18}:0** adlayer is the most stable phase over a wide concentration range. However, at 1:10 mol ratio, the cocrystal coexists with the phase-pure 2D crystal of the saturated amide. The cocrystal thus appears to be an intermediate phase that prevails on the surface until the mole ratio is favorable for the formation of the high energy **C_{18}:$1c_9$** phase. It must be noted at this juncture that, on going from 1:1 to 1:10 mole ratio, the concentration of the **C_{18}:$1c_9$** amide is always more than sufficient to form a complete monolayer of phase-pure **C_{18}:$1c_9$**. Despite this fact, the cocrystal phase is favored

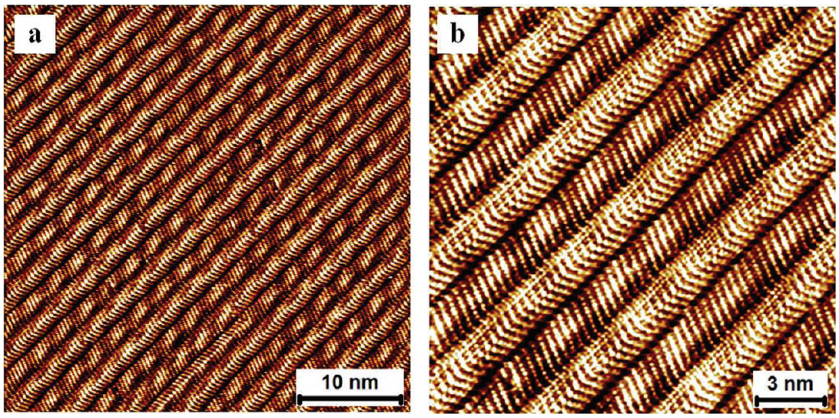

Figure 7. Large-scale (a) and high-resolution (b) STM image obtained after annealing the sample at 70 °C for 25 min. It can be clearly noticed that the cocrystal survives the annealing step and relatively larger domains of flawless cocrystal evolve. Imaging conditions: I_{set} = 368 pA, V_{bias} = −367 mV.

(above 1:10) and only individual phase-separated columns are observed (occasionally) on the surface, which indicates that the cocrystal is more stable than the phase-pure **C_{18}:1c_9** adlayer.

It can be argued that the cocrystal is a kinetically trapped metastable phase, and if one gives enough time to the system to evolve, it might lead to the formation of phase-separated species. In fact, such kinetically trapped metastable adlayers and their transformation to thermodynamically stable forms have been observed in the recent past by employing STM.[78] Nevertheless, it must be noted that the noncovalent interactions involved in the self-assembly process at the liquid−solid interface are highly reversible and thus generally warrant the optimum conditions to achieve equilibrium and hence favor the formation of thermodynamically stable structures. One can qualitatively ensure the formation of stable structures in the present case by heating the sample (mole ratio 1:10) at elevated temperatures, thus imparting enough energy to the molecules on the surface so that they can find their "right" partners and drive the system toward an equilibrated state. Therefore, the stability of the cocrystal was examined by heating the sample *ex-situ* at 70 °C for 25 min in a liquid cell prior to imaging. The outcome of such experiments reveals that annealing in fact promotes the formation of relatively larger domains of flawless cocrystallized phase and reduces the number and size of phase-separated **C_{18}:1c_9** columns (Figure 7), which also confirms the stability of the cocrystal relative to the phase-pure adlayer of **C_{18}:1c_9**. Thus, the formation of cocrystal with increasing proportion of **C_{18}:1c_9** can be considered as an energetic compromise in response to the change in the solution composition.

The argument presented in the previous paragraph is further supported by the total potential energies obtained from MD simulations of the cocrystal (Table 4). A comparison of relative stabilities of *cis*-unsaturated and saturated parts of the cocrystal is provided in the Supporting Information. The differences in the lattice stability combined with the changes in the solution composition thus promote the cocrystal formation instead of phase separation. The rationalization presented here might appear to fall short if one considers the high lattice stability of the **C_{18}:0** adlayer itself. Although the phase separation of the **C_{18}:1c_9** adlayer is prevented in view of energetic constraint, that is not an issue for the phase separation of the **C_{18}:0** adlayer. Then the question is, why doesn't **C_{18}:0** phase separate completely, leaving behind domains of **C_{18}:1c_9** molecules? To address this issue, one must consider the following fundamental aspects of the self-assembly process. Self-assembly at the liquid−solid interface is controlled by the interplay of adsorbate−adsorbate, adsorbate−substrate, adsorbate−solvent, and solvent−substrate interactions. The assembly process is dynamic and depends on the adsorption−desorption equilibrium. In the present case, if the saturated amide phase separates and forms a domain by itself, it will maximize the molecule−molecule and molecule−substrate interactions. On the other hand, this situation will lead to concomitant phase separation of the *cis*-amide, which has substantially low molecule−molecule and molecule−substrate interactions due to decreased van der Waals contact.

However, if one considers the total free energy gain of the system in the phase separation scenario, the energy gain by phase separation of one species (**C_{18}:0**) will be more or less compensated by the energy loss by the phase separation process of the other (**C_{18}:1c_9**). Thus, to maximize the overall free energy of the system at a given (high) mole ratio, the cocrystal formation is favored over phase separation. To the best of our knowledge, this is the first example wherein linear saturated and bent unsaturated rodlike molecules are cocrystallized and visualized with high spatial resolution using STM. Considering the increasing popularity of the cocrystallization processes in the pharmaceutical industry in the recent past, the present example of cocrystallization

of "shap-incompatible" molecules could be a relevant and interesting strategy.

CONCLUSIONS

Formation of 2D crystallized adlayers at interfaces is one of the simple means of producing ever-more-complex surface patterns. Besides their technological importance, such surface-confined molecular patterns can be employed as model systems for isolating and understanding the factors that complicate bulk crystallizations. We have employed a reductionist's approach to scrutinize the 2D crystallization and mixing behavior of "shape-compatible" as well as "shape-incompatible" alkylamides at the liquid−solid interface by using a combination of STM, DSC, and computational modeling. The 2D crystal structures of the phase-pure adlayers of saturated and unsaturated alkylamides have been established at submolecular resolution by employing STM. Furthermore, the two-component 2D phase behavior of the binary mixtures of alkylamides was investigated in detail at the liquid−solid interface. The saturated and *trans*-unsaturated amides were found to mix ideally on the surface in view of their size and shape compatibility. The 2D crystal composition showed marked dependence on the solution mole ratio, which could be used to control the crystalline packing at the liquid−solid interface. The *cis*-unsaturated amides were found to mix surprisingly well with saturated amides, which are essentially straight molecules. This mixing behavior is rather unexpected in view of the "shape-incompatibility" of the two molecules, combined with the stringent constraints imposed by the 2D nature of the problem. Despite this fact, the molecules could clearly find packings where they coexist on the surface *via* formation of cocrystals. The cocrystal formation is a manifestation of a combination of different factors such as relative lattice energies in 2D, strong intermolecular interactions, and, more importantly, energetic compromises to accommodate the changes in the solution composition. The results presented here clearly demonstrate that it is possible to direct the 2D cocrystallization of molecular components on surfaces that do not strictly comply with the shape complementarity rule. Identification of such novel modes of 2D cocrystallization of materials may have important implications in understanding the behavior of complex and commercially important thin film materials as well as in the rational design of solid-state materials for interfacial applications.

MATERIALS AND METHODS

STM Measurements. The amides used in this work were synthesized from the corresponding carboxylic acids (Sigma-Aldrich) as described previously.[79] The purities of the amides were assessed by a combination of ^{1}H NMR, liquid chromatography/mass spectrometry, and elemental analysis, and all the amides were found to be reasonably pure (>96%). Stock solutions of the three amides were prepared by dissolving approximately 1.0 mg of solid per 2 g of 1-phenyloctane (Aldrich, 98%). The typical concentrations of the stock solutions are in the range $(1.0-1.5) \times 10^{-3}$ M. Binary mixtures with different mole ratios of the amides were prepared by mixing appropriate volumes of these stock solutions. The final concentrations of the mixed solutions were kept constant to allow comparison between different mole ratios. ($[\mathbf{C_{18}{:}0}+\mathbf{C_{18}{:}1t_9}] \approx 1.3 \times 10^{-3}$ M, whereas $[\mathbf{C_{18}{:}0}+\mathbf{C_{18}{:}1c_9}] \approx 1.6 \times 10^{-3}$ M). All STM experiments were performed at room temperature (20−23 °C) using a PicoLE (Agilent) machine operating in constant-current mode with the tip immersed in the supernatant liquid. STM tips were prepared by mechanical cutting from Pt/Ir wire (80%/20%, diameter 0.2 mm). Prior to imaging, a drop of the amide solution was applied onto a freshly cleaved surface of highly oriented pyrolytic graphite (HOPG, grade ZYB, Advanced Ceramics Inc., Cleveland, OH, USA). The experiments were repeated in several sessions using different tips to check for reproducibility and to avoid experimental artifacts, if any. For analysis purposes, recording of a monolayer image was followed by imaging the graphite substrate underneath it under the same experimental conditions, except for lowering the bias. The images were corrected for drift *via* scanning probe image processor (SPIP) software (Image Metrology ApS), using the recorded graphite images for calibration purposes, allowing a more accurate unit cell determination. The unit cell parameters were determined by examining at least 10 images, and only the average values are reported. The images are low-pass filtered. The imaging parameters are indicated in the figure caption: tunneling current (I_{set}) and sample bias (V_{bias}).

Molecular Modeling. A molecular mechanics/molecular dynamics (MM/MD) approach was used to estimate the energetics of 2D layers and their relative stability. The Dreiding force field,[80] as implemented in the Forcite tool pack of Materials Studio, was used since it is particularly adapted to account for the hydrogen bonds that drive the assembly. The modeling was performed on a frozen graphite slab of 19.6 × 19.6 nm (parallelogram shape). The simulations on the "pure" components consisted of six rows of 16 amide molecules. In the "mixed" systems, we considered the 1:1 ratio in all cases (cocrystal I, cocrystal II, and phase-separated for mixtures of saturated and *cis*- unsaturated amides; cocrystal, phase-separated, and random mixtures of saturated and *trans*-unsaturated amides) using four rows of 16 amide molecules. The initial geometries, built on the basis of the STM observations, were submitted to energy minimization at 0 K, followed by MD simulations in the NVT ensemble at 298 K for 1 ns (the energies presented in the different tables are extracted from the MD simulations). The energies are given in kJ mol^{-1} molecule^{-1}. The long-range nonbonded interactions were turned off with a cubic spline cutoff set at 18 Å.

Acknowledgment. This work is supported by the Fund of Scientific Research−Flanders (FWO), K.U. Leuven (GOA 2006/2), and Belgian Federal Science Policy Office (IAP-6/27). The authors thank the Nehru Trust of Cambridge University and Diamond Light Source, U.K., for financial assistance and C. N. Sporikou for help with synthesis of the amides. Research in Mons is supported by Région Wallonne (OPTI2MAT Excellence Programme) and FNRS-FRFC.

Supporting Information Available: (1) Additional schematics and STM images of the monocomponent as well as bicomponent systems. (2) Details of the computational models. This material is available free of charge *via* the Internet at http://pubs.acs.org.

REFERENCES AND NOTES

1. Desiraju, G. R. Cryptic Crystallography. *Nat. Mater.* **2002**, *1*, 77–79.
2. Woodley, S. M.; Catlow, R. Crystal Structure Prediction from First Principles. *Nat. Mater.* **2008**, *7*, 937–946.
3. Dunitz, J. D. Are Crystal Structures Predictable? *Chem Commun.* **2003**, 545–548.
4. Elemans, J. A. A. W.; Lei, S. B.; De Feyter, S. Molecular and Supramolecular Networks on Surfaces: From Two-Dimensional Crystal Engineering to Reactivity. *Angew. Chem., Int. Ed.* **2009**, *48*, 7298–7332.
5. Wan, L. J. Fabricating and Controlling Molecular Self-Organization at Solid Surfaces: Studies by Scanning Tunneling Microscopy. *Acc. Chem. Res.* **2006**, *39*, 334–342.
6. Lei, S. B.; Tahara, K.; Adisoejoso, J.; Balandina, T.; Tobe, Y.; De Feyter, S. Towards Two-Dimensional Nanoporous Networks: Crystal Engineering at the Solid−Liquid Interface. *CrystEngComm* **2010**, *12*, 3369–3381.
7. Ciesielski, A.; Palma, C. A.; Bonini, M.; Samorì, P. Towards Supramolecular Engineering of Functional Nanomaterials: Pre-Programming Multi-Component 2D Self-Assembly at Solid-Liquid Interfaces. *Adv. Mater.* **2010**, *22*, 3506–3520.
8. Bonifazi, D.; Mohnani, S.; Llanes-Pallas, A. Supramolecular Chemistry at Interfaces: Molecular Recognition on Nanopatterned Porous Surfaces. *Chem.—Eur. J.* **2009**, *15*, 7004–7025.
9. Bonini, M.; Zalewski, L.; Breiner, T.; Dotz, F.; Kastler, M.; Schadler, V.; Surin, M.; Lazzaroni, R.; Samorì, P. Competitive Physisorption Among Alkyl-Substituted π-Conjugated Oligomers at the Solid−Liquid Interface: Towards Prediction of Self-assembly at Surfaces from a Multicomponent Solution. *Small* **2009**, *5*, 1521–1526.
10. Hines, J. D.; Thomas, R. K.; Garrett, P. R.; Rennie, G. K.; Penfold, J. Investigation of Mixing in Binary Surfactant Solutions by Surface Tension and Neutron Reflection: Anionic/Nonionic and Zwitterionic/Nonionic Mixtures. *J. Phys. Chem. B* **1997**, *101*, 9215–9223.
11. Clarke, S. M. Neutron Diffraction and Incoherent Neutron Scattering from Adsorbed Layers. *Curr. Opin. Colloid. Interfaces* **2001**, *6*, 118–125.
12. Bhinde, T.; Clarke, S. M.; Phillips, T. K.; Arnold, T.; Parker, J. E. Crystalline Structures of Alkylamide Monolayers Adsorbed on the Surface of Graphite. *Langmuir* **2010**, *26*, 8201–8206.
13. Sun, C.; Bojdys, M. J.; Clarke, S. M.; Harper, L. D.; Jefferson, A.; Castro, M. A.; Medina, S. Bulk and Adsorbed Monolayer Phase Behavior of Binary Mixtures of Undecanoic Acid and Undecylamine: Catanionic Monolayers. *Langmuir* **2011**, *27*, 3626–3637.
14. De Feyter, S.; De Schryver, F. C. Self-Assembly at the Liquid/Solid Interface: STM Reveals. *J. Phys. Chem. B* **2005**, *109*, 4290–4302.
15. Deacon, R. F.; Goodman, J. F. Lubrication by Lamellar Solids. *Proc. R. Soc. London, Ser. A* **1958**, *243*, 464–482.
16. Butt, H.-J.; Graf, K.; Kappl, M. In *Physics and Chemistry of Interfaces*, 2nd., rev. and enl. ed.; Wiley-VCH: Weinheim, 2006.
17. Mativetsky, J. M.; Kastler, M.; Savage, R. C.; Gentilini, D.; Palma, M.; Pisula, W.; Mullen, K.; Samorì, P. Supramolecular Self-Assembly: Self-Assembly of A Donor-Acceptor Dyad across Multiple Length Scales: Functional Architectures for Organic Electronics. *Adv. Funct. Mater.* **2009**, *19*, 2486–2494.
18. Cowie, J. M. G.; Arrighi, V. In *Polymers: Chemistry and Physics of Modern Materials*, 3rd ed.; CRC Press: Boca Raton, FL, 2008.
19. Elbel, N.; Roth, W.; Gunther, E.; Vonseggern, H. STM Imaging of Coadsorption Phenomena and Molecular Dynamics in Mixed Alcanol Monolayers. *Surf. Sci.* **1994**, *303*, 424–432.
20. Venkataraman, B.; Breen, J. J.; Flynn, G. W. Scanning Tunneling Microscopy Studies of Alcohol/Alkane Mixtures Adsorbed on Graphite Surfaces. In *Atomic Force Microscopy/Scanning Tunneling Microscopy*; Cohen, S. H.; Bray, M. T.; Lightbody, M. L., Eds.; Plenum Press: New York, 1994; pp 117−125.
21. Venkataraman, B.; Breen, J. J.; Flynn, G. W. Scanning Tunneling Microscopy Studies of Solvent Effects on the Adsorption and Mobility of Triacontane/Triacontanol Molecules Adsorbed on Graphite. *J. Phys. Chem.* **1995**, *99*, 6608–6619.
22. Baker, R. T.; Mougous, J. D.; Brackley, A.; Patrick, D. L. Competitive Adsorption, Phase Segregation, and Molecular Motion at A Solid−Liquid Interface Studied by Scanning Tunneling Microscopy. *Langmuir* **1999**, *15*, 4884–4891.
23. Kim, K.; Plass, K. E.; Matzger, A. J. Structure of and Competitive Adsorption in Alkyl Dicarbamate Two-Dimensional Crystals. *J. Am. Chem. Soc.* **2005**, *127*, 4879–4887.
24. Palma, C. A.; Bjork, J.; Bonini, M.; Dyer, M. S.; Llanes-Pallas, A.; Bonifazi, D.; Persson, M.; Samorì, P. Tailoring Bicomponent Supramolecular Nanoporous Networks: Phase Segregation, Polymorphism, and Glasses at the Solid−Liquid Interface. *J. Am. Chem. Soc.* **2009**, *131*, 13062–13071.
25. Hipps, K. W.; Lu, X.; Wang, X. D.; Mazur, U. Metal d-Orbital Occupation-Dependent Images in the Scanning Tunneling Microscopy of Metal Phthalocyanines. *J. Phys. Chem.* **1996**, *100*, 11207–11210.
26. Lu, X.; Hipps, K. W.; Wang, X. D.; Mazur, U. Scanning Tunneling Microscopy of Metal Phthalocyanines: D^7 and D^9 Cases. *J. Am. Chem. Soc.* **1996**, *118*, 7197–7202.
27. Tao, N. J. Probing Potential-Tuned Resonant Tunneling Through Redox Molecules with Scanning Tunneling Microscopy. *Phys. Rev. Lett.* **1996**, *76*, 4066–4069.
28. Gesquiere, A.; Abdel-Mottaleb, M. M.; De Schryver, F. C.; Sieffert, M.; Mullen, K. Imaging of A Fluorine-Substituted Isophthalic Acid Derivative on Graphite with Scanning Tunneling Microscopy. *Langmuir* **1999**, *15*, 6821–6824.
29. Stevens, F.; Beebe, T. P. Dynamical Exchange Behavior in Organic Monolayers Studied by STM Analysis of Labeled Mixtures. *Langmuir* **1999**, *15*, 6884–6889.
30. Padowitz, D. F.; Messmore, B. W. STM Observations of Exchange Dynamics at the Solid−Liquid Interface Using a Molecular Tracer. *J. Phys. Chem. B* **2000**, *104*, 9943–9946.
31. Padowitz, D. F.; Sada, D. M.; Kemer, E. L.; Dougan, M. L.; Xue, W. A. Molecular Tracer Dynamics in Crystalline Organic Films at the Solid−Liquid Interface. *J. Phys. Chem. B* **2002**, *106*, 593–598.
32. Xie, Z. X.; Xu, X.; Mao, B. W.; Tanaka, K. Self-Assembled Binary Monolayers of *n*-Alkanes on Reconstructed Au(111) and HOPG Surfaces. *Langmuir* **2002**, *18*, 3113–3116.
33. Ahn, S.; Matzger, A. J. Anatomy of One-Dimensional Cocrystals: Randomness into Order. *J. Am. Chem. Soc.* **2009**, *131*, 13826–13832.
34. Ciesielski, A.; Lena, S.; Masiero, S.; Spada, G. P.; Samorì, P. Dynamers at the Solid−Liquid Interface: Controlling the Reversible Assembly/Reassembly Process Between Two Highly Ordered Supramolecular Guanine Motifs. *Angew. Chem., Int. Ed.* **2010**, *49*, 1963–1966.
35. Eichhorst-Gerner, K.; Stabel, A.; Moessner, G.; Declerq, D.; Valiyaveettil, S.; Enkelmann, V.; Mullen, K.; Rabe, J. P. Self-Assembly of A Two-Component Hydrogen-Bonded Network: Comparison of the Two-Dimensional Structure Observed by Scanning Tunneling Microscopy and the Three-Dimensional Crystal Lattice. *Angew. Chem., Int. Ed. Engl.* **1996**, *35*, 1492–1495.
36. Gesquiere, A.; Abdel-Mottaleb, M. M.; De Feyter, S.; De Schryver, F. C.; Sieffert, M.; Mullen, K.; Calderone, A.; Lazzaroni, R.; Bredas, J. L. Dynamics in Physisorbed Monolayers of 5-Alkoxy-Isophthalic Acid Derivatives at the Liquid/Solid Interface Investigated by Scanning Tunneling Microscopy. *Chem.—Eur. J.* **2000**, *6*, 3739–3746.
37. Grim, P. C. M.; De Feyter, S.; Gesquiere, A.; Vanoppen, P.; Rucker, M.; Valiyaveettil, S.; Moessner, G.; Mullen, K.; De Schryver, F. C. Supramolecularly Resolved Polymerization of Diacetylene Molecules on the Graphite Surface Observed with Scanning Tunneling Microscopy. *Angew. Chem., Int. Ed. Engl.* **1997**, *36*, 2601–2603.
38. Hipps, K. W.; Scudiero, L.; Barlow, D. E.; Cooke, M. P. A Self-Organized 2-Dimensional Bifunctional Structure Formed

by Supramolecular Design. *J. Am. Chem. Soc.* **2002**, *124*, 2126–2127.
39. Kampschulte, L.; Werblowsky, T. L.; Kishore, R. S. K.; Schmittel, M.; Heckl, W. M.; Lackinger, M. Thermodynamical Equilibrium of Binary Supramolecular Networks at the Liquid–Solid Interface. *J. Am. Chem. Soc.* **2008**, *130*, 8502–8507.
40. Mali, K. S.; Lava, K.; Binnemans, K.; De Feyter, S. Hydrogen Bonding *versus* Van Der Waals Interactions: Competitive Influence of Noncovalent Interactions on 2D Self-Assembly at the Liquid–Solid Interface. *Chem.—Eur. J.* **2010**, *16*, 14447–14458.
41. Mamdouh, W.; Dong, M. D.; Xu, S. L.; Rauls, E.; Besenbacher, F. Supramolecular Nanopatterns Self-Assembled by Adenine–Thymine Quartets at the Liquid/Solid Interface. *J. Am. Chem. Soc.* **2006**, *128*, 13305–13311.
42. Mamdouh, W.; Kelly, R. E. A.; Dong, M. D.; Kantorovich, L. N.; Besenbacher, F. Two-Dimensional Supramolecular Nanopatterns Formed by the Coadsorption of Guanine and Uracil at the Liquid/Solid Interface. *J. Am. Chem. Soc.* **2008**, *130*, 695–702.
43. Nath, K. G.; Ivasenko, O.; Miwa, J. A.; Dang, H.; Wuest, J. D.; Nanci, A.; Perepichka, D. F.; Rosei, F. Rational Modulation of the Periodicity in Linear Hydrogen-Bonded Assemblies of Trimesic Acid on Surfaces. *J. Am. Chem. Soc.* **2006**, *128*, 4212–4213.
44. Plass, K. E.; Engle, K. M.; Cychosz, K. A.; Matzger, A. J. Large-Periodicity Two-Dimensional Crystals by Cocrystallization. *Nano Lett.* **2006**, *6*, 1178–1183.
45. Schull, G.; Douillard, L.; Fiorini-Debuisschert, C.; Charra, F.; Mathevet, F.; Kreher, D.; Attias, A. J. Single-Molecule Dynamics in a Self-Assembled 2D Molecular Sieve. *Nano Lett.* **2006**, *6*, 1360–1363.
46. Tao, F.; Bernasek, S. L. Two-Dimensional Self-Assembly of a Two-Component Molecular System: Formation of an Ordered and Homogeneous Molecular Mesh. *J. Am. Chem. Soc.* **2005**, *127*, 12750–12751.
47. Vanoppen, P.; Grim, P. C. M.; Rucker, M.; DeFeyter, S.; Moessner, G.; Valiyaveettil, S.; Mullen, K.; DeSchryver, F. C. Solvent Codeposition and *Cis–Trans* Isomerization of Isophthalic Acid Derivatives Studied by STM. *J. Phys. Chem.* **1996**, *100*, 19636–19641.
48. Wang, G. J.; Lei, S. B.; De Feyter, S.; Feldman, R.; Parker, J. E.; Clarke, S. M. Behavior of Binary Alcohol Mixtures Adsorbed on Graphite Using Calorimetry and Scanning Tunneling Microscopy. *Langmuir* **2008**, *24*, 2501–2508.
49. Yang, X. Y.; Mu, Z. C.; Wang, Z. Q.; Zhang, X.; Wang, J.; Wang, Y. STM Study on Quinacridone Derivative Assemblies: Modulation of the Two-Dimensional Structure by Coadsorption with Dicarboxylic Acids. *Langmuir* **2005**, *21*, 7225–7229.
50. Adisoejoso, J.; Tahara, K.; Okuhata, S.; Lei, S.; Tobe, Y.; De Feyter, S. Two-Dimensional Crystal Engineering: A Four-Component Architecture at a Liquid–Solid Interface. *Angew. Chem., Int. Ed.* **2009**, *48*, 7353–7357.
51. Shen, Y.; Zeng, L.; Lei, D.; Zhang, X.; Deng, K.; Feng, Y.; Feng, W.; Lei, S.; Li, S.; Gan, L.; *et al*. Competitive Adsorption and Dynamics of Guest Molecules in 2D Molecular Sieves. *J. Mater. Chem.* **2011**, *21*, 8787–8791.
52. Shen, Y.-T.; Deng, K.; Zhang, X.-M.; Feng, W.; Zeng, Q.-D.; Wang, C.; Gong, J. R. Switchable Ternary Nanoporous Supramolecular Network on Photo-Regulation. *Nano Lett.* **2011**, *11*, 3245–3250.
53. Messe, L.; Clarke, S. M.; Arnold, T.; Dong, C.; Thomas, R. K.; Inaba, A. Mixing Behavior at the Solid/Liquid Interface: Binary Monolayers of Linear Alcohols Adsorbed on Graphite. *Langmuir* **2002**, *18*, 4010–4013.
54. Clarke, S. M.; Friscic, T.; Jones, W.; Mandal, A.; Sun, C. G.; Parker, J. E. Observation of a Two-Dimensional Halogen-Bonded Cocrystal at Sub-Monolayer Coverage using Synchrotron X-Ray Diffraction. *Chem. Commun.* **2011**, *47*, 2526–2528.
55. Clarke, S. M.; Messe, L.; Adams, J.; Inaba, A.; Arnold, T.; Thomas, R. K. A Quantitative Parameter for Predicting Mixing Behaviour in Adsorbed Layers: The 2D Isomorphism Coefficient. *Chem. Phys. Lett.* **2003**, *373*, 480–485.
56. Ramirez, M. X.; Hirt, D. E.; Wright, L. L. AFM Characterization of Surface Segregated Erucamide and Behenamide in Linear Low Density Polyethylene Film. *Nano Lett.* **2002**, *2*, 9–12.
57. Arnold, T.; Clarke, S. M. Thermodynamic Investigation of the Adsorption of Amides on Graphite from their Liquids and Binary Mixtures. *Langmuir* **2008**, *24*, 3325–3335.
58. Feng, C. L.; Zhang, Y. J.; Jin, J.; Song, Y. L.; Xie, L. Y.; Qu, G. R.; Jiang, L.; Zhu, D. B. Completely Interfacial Photoisomerization of 4-Hydroxy-3′-Trifluoromethyl-Azobenzene Studied by STM on HOPG. *Surf. Sci.* **2002**, *513*, 111–118.
59. Bleger, D.; Ciesielski, A.; Samorì, P.; Hecht, S. Photoswitching Vertically Oriented Azobenzene Self-Assembled Monolayers at the Solid–Liquid Interface. *Chem.—Eur. J.* **2010**, *16*, 14256–14260.
60. Tao, F.; Goswami, J.; Bernasek, S. L. Self-Assembly and Odd–Even Effects of *cis*-Unsaturated Carboxylic Acids on Highly Oriented Pyrolytic Graphite. *J. Phys. Chem. B* **2006**, *110*, 4199–4206.
61. Ueno, S.; Suetake, T.; Yano, J.; Suzuki, M.; Sato, K. Structure and Polymorphic Transformations in Elaidic Acid (*trans*-ω9-octadecenoic acid). *Chem. Phys. Lipids* **1994**, *72*, 27–34.
62. Brown, D. A.; London, E. Structure and Function of Sphingolipid- and Cholesterol-rich Membrane Rafts. *J. Biol. Chem.* **2000**, *275*, 17221–17224.
63. Brown, D. A.; London, E. Structure and Origin of Ordered Lipid Domains in Biological Membranes. *J. Membr. Biol.* **1998**, *164*, 103–114.
64. Rietveld, A.; Simons, K. the Differential Miscibility of Lipids as the Basis for the Formation of Functional Membrane Rafts. *Bba-Rev. Biomembranes* **1998**, *1376*, 467–479.
65. Pimentel, G. C.; McClellan, A. L. In *The Hydrogen Bond*; Freeman, W. H., Ed.; Reinhold Pub. Corp.: New York, 1960.
66. Vinogradov, S. N.; Linnell, R. H. *Hydrogen Bonding*; Van Nostrand Reinhold: New York, 1971.
67. Messe, L.; Perdigon, A.; Clarke, S. M.; Inaba, A.; Arnold, T. Alkane/Alcohol Mixed Monolayers at the Solid/Liquid Interface. *Langmuir* **2005**, *21*, 5085–5093.
68. Giancarlo, L.; Cyr, D.; Muyskens, K.; Flynn, G. W. Scanning Tunneling Microscopy of Molecular Adsorbates at the Liquid–Solid Interface: Functional Group Variations in Image Contrast. *Langmuir* **1998**, *14*, 1465–1471.
69. Ilan, B.; Florio, G. M.; Hybertsen, M. S.; Berne, B. J.; Flynn, G. W. Scanning Tunneling Microscopy Images of Alkane Derivatives on Graphite: Role of Electronic Effects. *Nano Lett.* **2008**, *8*, 3160–3165.
70. Rabe, J. P.; Buchholz, S. Commensurability and Mobility in Two-Dimensional Molecular Patterns on Graphite. *Science* **1991**, *253*, 424–427.
71. Claypool, C. L.; Faglioni, F.; Goddard, W. A.; Gray, H. B.; Lewis, N. S.; Marcus, R. A. Source of Image Contrast in STM Images of Functionalized Alkanes on Graphite: A Systematic Functional Group Approach. *J. Phys. Chem. B* **1997**, *101*, 5978–5995.
72. Hibino, M.; Sumi, A.; Hatta, I. Atomic Images of Saturated and Unsaturated Fatty Acids at Liquid/Graphite Interface and Difference of Tunneling Currents between them Observed by Scanning Tunneling Microscopy. *Jpn. J. Appl. Phys. 1* **1995**, *34*, 610–614.
73. The monolayer melting points of the three systems are $\mathbf{C_{18}{:}0}$ = 433 ± 7 K, $\mathbf{C_{18}{:}1t_9}$ = 415 ± 1.5 K, $\mathbf{C_{18}{:}1c_9}$ = 399 ± 5 K.
74. Xia, T. K.; Landman, U. Molecular Dynamics of Adsorption and Segregation from an Alkane Mixture. *Science* **1993**, *261*, 1310–1312.
75. Castro, M. A.; Clarke, S. M.; Inaba, A.; Thomas, R. K.; Thomas, A. Preferential Adsorption from Binary Mixtures of Short Chain *n*-Alkanes; The Octane–Decane System. *J. Phys. Chem. B* **2001**, *105*, 8577–8582.
76. Yablon, D. G.; Ertas, D.; Fang, H.; Flynn, G. W. An STM Investigation of the Adsorption of Mixtures of Fatty Acids and Substituted Acids at the Solution-Graphite Interface. *Isr. J. Chem.* **2003**, *43*, 383–392.
77. Wintersmith, J. R.; Zou, L.; Bernoff, A. J.; Alexander, J. C.; Mann, J. A.; Kooijman, E. E.; Mann, E. K. Determination of

Interphase Line Tension in Langmuir Films. *Phys. Rev. E* **2007**, *75*, 0616051–0616056.
78. Kim, K.; Plass, K. E.; Matzger, A. J. Kinetic and Thermodynamic Forms of a Two-Dimensional Crystal. *Langmuir* **2003**, *19*, 7149–7152.
79. Kent, R. E.; McElvain, S. M. *Organic Syntheses*; Wiley: New York, 1955; Collect. Vol. 3, pp 490–492.
80. Mayo, S. L.; Olafson, B. D.; Goddard, W. A. DREIDING: A Generic Force Field for Molecular Simulations. *J. Phys. Chem.* **1990**, *94*, 8897–8909.